

- jet for laser/cluster interaction experiments. *Rev. Sci. Instrum.* **69**, 3798–3804 (1998).
23. Klingelhöfer, R. & Moser, H. O. Production of large hydrogen clusters in condensed molecular beams. *J. Appl. Phys.* **43**, 4575–4579 (1972).
24. Ditmire, T., Smith, R. A., Tisch, J. W. G. & Hutchinson, M. H. R. Absorption of high intensity laser pulses in gases of clusters. *Phys. Rev. Lett.* **78**, 3121–3124 (1997).
25. Shigemori, K. *et al.* Measurement of strong blast waves in gas cluster targets. *Ap. J. Lett.* (submitted).
26. Teller, E. *Fusion* (Academic, New York, 1981).
27. Zweiback, J., Ditmire, T. & Perry, M. D. Femtosecond time resolved studies of the dynamics of noble gas cluster explosions. *Phys. Rev. Lett. A* (in the press).
28. Loveman, R., Bendahan, J., Gozani, T. & Stevenson, J. Time-of-flight fast-neutron radiography. *Nucl. Instrum. Meth. Phys. Res. B: Beam Interact. Mater. Atoms* **99**, 765–768 (1995).

Acknowledgements. We thank R. Smith, J. Tisch and other collaborators from Imperial College for many useful conversations; M. Perry and H. Powell for useful input; and V. Tsai for technical assistance.

Correspondence and requests for materials should be addressed to T.D. (e-mail: ditmire1@lnl.gov).

Thermodynamic determination of fragility in liquids and a fragile-to-strong liquid transition in water

Kaori Ito*, Cornelius T. Moynihan† & C. Austen Angell‡

* Department of Biotechnology, Tokyo University of Agriculture and Technology, Koganei, Tokyo, 184-8588, Japan

† Materials Science and Engineering Department, Rensselaer Polytechnic Institute, Troy, New York 12180, USA

‡ Chemistry Department, Arizona State University, Tempe, Arizona 85287, USA

If crystallization can be avoided when a liquid is cooled, it will typically form a glass. Near the glass transition temperature the viscosity increases continuously but rapidly with cooling. As the glass forms, the molecular relaxation time increases with an Arrhenius-like (simple activated) form in some liquids, but shows highly non-Arrhenius behaviour in others. The former are said to be ‘strong’ liquids, and the latter ‘fragile’^{1,2}. Here we show that the fragility of a liquid can be determined from purely thermodynamic data (as opposed to measurements of kinetics) near and below the melting point. We find that for most liquids the fragilities estimated this way are consistent with those obtained by previous methods and by a new method (ref. 3 and K.I., C.A.A. and C.T.M., unpublished data) at temperatures near the glass transition. But water is an exception. The thermodynamic method indicates that near its melting point it is the most fragile of all liquids studied, whereas the kinetic approach indicates that near the glass transition it is the least fragile. We propose that this discrepancy can be explained by a fragile-to-strong transition in supercooled water near 228 K, corresponding to a change in the liquid’s structure at this point.

One of the intriguing (and still unresolved) questions about supercooled liquids was posed in 1948 by Kauzmann⁴, who showed that many liquids lose entropy on supercooling so much faster than the corresponding crystalline phase that an ‘entropy crisis’, where $S_{liq} < S_{cryst}$, should occur at temperatures as high as $0.67T_m$ (here S_{liq} and S_{cryst} are the entropies in the liquid and the crystal, respectively, and T_m is the melting point). This situation is averted only by the occurrence of the glass transition. The entropy crisis is most pressing for the fragile liquids. We reproduce in Fig. 1 Kauzmann’s plot of the entropy difference ΔS between the liquid and the crystal normalized to the entropy difference at the melting point, $\Delta S/\Delta S_m$, versus normalized temperature T/T_m . Newer data have been added for the very fragile salt hydrate, $Ca(NO_3)_2 \cdot 4H_2O$ (refs 5–7), for the less fragile molecular liquid bromopentane^{8,9}, and for the rather strong covalent liquid As_2Se_3 (refs 2, 10 and S. S. Chang, personal communication). The temperature where $\Delta S/\Delta S_m \rightarrow 0$ by extrapolation, known as the Kauzmann temperature T_K , is the effective ground-state temperature for each liquid. Consistent

with the idea of fragility as a rate-of-structural-change metric, the liquids that on cooling approach their T_K most rapidly are seen also to be the liquids in the original ‘fragility plot’^{1,2} whose viscosities, plotted against T_g/T , approach infinity most rapidly (here T_g is the glass transition temperature).

The correspondence of fragilities based, alternatively, on kinetic properties with those based on purely thermodynamic properties, is consistent with the notion advanced by Gibbs¹¹ and Goldstein¹² that the dynamics of liquids largely reflect the underlying thermodynamics of the liquid state. This idea has recently been strongly supported by the ‘inherent structure’ or ‘landscape’ analysis of Sastry *et al.*¹³, for a model system studied by computer simulation. Figure 1 has the advantage that it can include liquids which, like water, do not have good glass-forming ability owing to fast crystallization kinetics. Data for liquid water at temperatures down to $-35^\circ C$ (ref. 14) are included in Fig. 1. By the standard of Fig. 1, water is seen to be the most fragile liquid of all, notwithstanding a subtle effect which makes easily crystallizing liquids appear less fragile than they would on the normal (T_g -scaled) ‘fragility plot’.

The nature of the data in Fig. 1 invites fragility for glass-formers to be quantified by the ratio T_g/T_K , by analogy with the metric $F = T_o/T_g$ (where T_o is the relaxation time divergence temperature of the Vogel–Fulcher–Tammann equation) suggested by some authors^{15,16} for relaxation-based (kinetic) fragilities. An ambiguity which is common to these two fragility metrics arises from the need for extrapolations to obtain T_K and T_o . The ambiguity can be removed in each case by defining $F_{1/2}$ fragilities. In the case based on relaxation time, $F_{1/2}$ has been defined⁹ using the temperature $T_{1/2}$ at which the relaxation time on a log scale is halfway between its

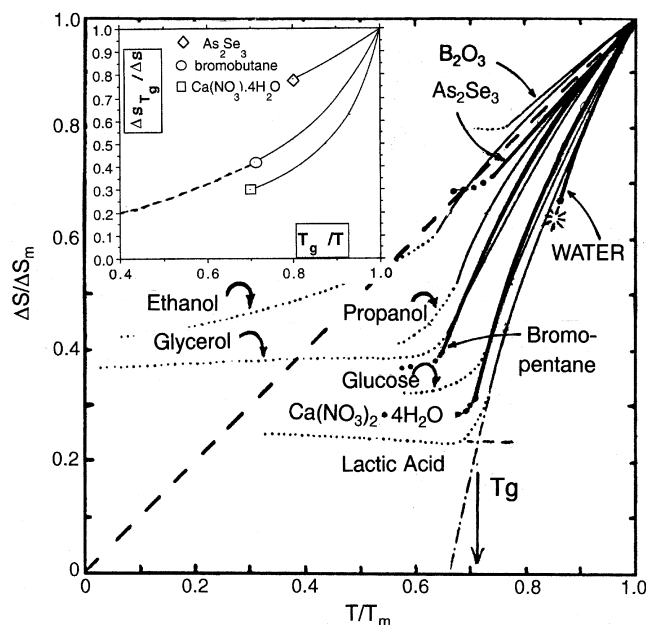


Figure 1 Use of the Kauzmann plot to define thermodynamic fragility for glass-forming liquids. The plot shows how the immediacy of the entropy crisis for liquids cooled below their melting temperatures follows the same order as the fragilities of these liquids as determined from the familiar T_g -scaled Arrhenius plot of transport data. Data for supercooled water on the same plot show the most fragile behaviour of all, despite a distortion towards lower fragility caused by the high melting-to-glass temperature ratio for water. The temperature of homogeneous nucleation for $\sim 2\text{-}\mu\text{m}$ emulsion droplets is marked by a star. Inset, alternative representation of data in main panel, which emphasizes the close relation of thermodynamic fragility to the more familiar (kinetic) fragility plot. Data for bromobutane were extended beyond the melting point in ref. 8. In this alternative plot, non-glassformers are excluded unless the scaling temperature T_g is obtained by estimation.

value at T_g ($\sim 10^2$ s) and the value at infinite temperature (phonon timescale) ($\sim 10^{-14}$ s). The definition, which gives fragility values between 0 and 1, is $F_{1/2} = 2(T_g/T_{1/2}) - 1$. A thermodynamic fragility, $F_{1/2,cal}$ (with values between zero and unity) can be likewise defined as $F_{1/2,cal} = T_{1/2}/T_m$, where $T_{1/2}/T_m$ is the T/T_m value where half the fusion entropy ΔS_m has been lost on cooling. However, "strong" glass-formers like B_2O_3 and As_2Se_3 can then only be included by extrapolation (see Fig. 1). An alternative and less ambiguous definition of thermodynamic fragility could be the fraction of the fusion entropy lost by $T/T_m = 0.8$, which can be determined experimentally for all the liquids in Fig. 1 except water. Water, by extrapolation, would have the highest fragility of the liquids shown in Fig. 1 (in fact it would be off-scale). Likewise, if we adopted the T_g implied by power-law fits of the various water relaxation data in the temperature range of the Fig. 1 entropy data, a uniquely high kinetic fragility, $F_{1/2}$, would be obtained for water. Even using the T_g value of 136 K obtained from calorimetric measurements on amorphous water—but which we will argue is inappropriate for the scaling of water data above 236 K—the fragility of water is high, though not uniquely so.

Before discussing the unusual properties of water in detail, we point out that, despite appearances, the data of Fig. 1 are effectively temperature-scaled by T_g , as in the common kinetic fragility plot. This is because, except for water, the substances in Fig. 1 obey the so-called "2/3 rule" of glass-formers, which says that T_g is approximately $(2/3)T_m$. Indeed, if the data of Fig. 1 are replotted in the form $\Delta S_{T_g}/\Delta S$ versus T_g/T , where ΔS_{T_g} is the value of ΔS at T_g , the resemblance to the standard fragility plot is striking, as shown in Fig. 1 inset. The establishment of a thermodynamic fragility scale for liquids, with its implications for the liquid density of states (vibrational and configurational)¹⁷, is an important objective of this work, but our main aim is to consider the unusual behaviour of water.

A glassy state of water would be expected to result from any cooling procedure that bypasses the crystallization at $0.85T_m$ (the star-burst symbol in Fig. 1). Assuming that such water followed the trend in Fig. 1 (increasing T_g/T_m with increasing steepness of the $\Delta S/\Delta S_m$ versus T/T_m plot), one would estimate for normal cooling rates near the glass transition that T_g for water would lie in the range roughly 200–220 K, depending on the chosen extrapolation of the (rapidly changing) liquid heat-capacity data used to calculate $\Delta S/\Delta S_m$. However, what is known from an abundance of binary solution glass-transition data^{18,19}, and from less definitive measurements on hyperquenched water itself^{20,21}, is that the glass transition of water is located at ~ 136 K. Furthermore, as we will show, the liquid which vitrifies at this temperature is a very strong liquid, notwithstanding binary solution extrapolations which predict the opposite¹⁹. Something strange happens to water on cooling between 236 and 150 K, or on addition of solutes at concentrations between zero and 20 mol%.

To demonstrate convincingly that water which has been obtained in the glassy state by very rapid cooling gives a kinetically "strong" liquid above its T_g , we need to obtain data on the temperature dependence of its structural relaxation time in this domain. This is usually obtained by some viscosity measurement or dielectric relaxation-time determination, but satisfactory data are not yet available for pure water. However, a simple alternative is available, as we will show below.

The glass transition is a relaxation phenomenon, and the decrease on cooling of the heat capacity from its equilibrium liquid value to the glassy value (and vice versa on reheating) occurs over a range of temperature; the range is determined primarily by how quickly the relaxation time changes with temperature. The transition extends over the temperature range needed to change the relaxation time by some 1.5–2.5 orders of magnitude^{3,22}, depending on the glass and on how the width of the glass transition is defined. A correlation of the glass transition width $\Delta T_g (= T'_g - T_g)$ from scanning calorimetry (Fig. 2, left inset) with the activation energy for viscosity η —which

is tantamount to a correlation of fragility with reduced glass transition width $\Delta T_g/T_g$ —has been demonstrated for inorganic glasses³. We have extended this correlation to molecular glasses using precise dielectric relaxation data instead of viscosities to define the $F_{1/2}$ fragilities. A combination of these results is shown in Fig. 2. The line shows the dependence of $\Delta T_g/T_g$ on $F_{1/2}$ predicted using the Vogel–Fulcher–Tammann equation for the temperature dependence of the relaxation time τ and the viscosity η ; this prediction uses the assumptions that the glass transition range ΔT_g (defined above) corresponds to a change of 2.3 decades in τ and η , and that τ and η at the onset T_g lie 16 decades above the microscopic (phonon) time τ_0 , and the high-temperature limit of η , as all the data indicate^{1,2}. Some details are given in Fig. 2 legend.

What can this tell us about water near its glass transition, generally identified as the low-density amorphous form of ice? We are particularly interested in the case of the material obtained by aerosol quenching of the liquid state, called HQG (hyper-quenched

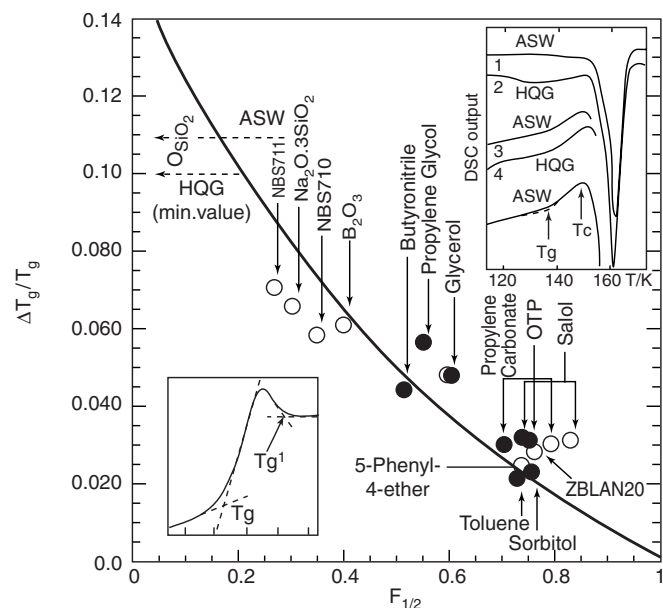


Figure 2 Correlation between fragility metrics $\Delta T_g/T_g$ and $F_{1/2}$. Shown is an extended correlation of the reduced glass transition width $\Delta T_g/T_g (= (T'_g - T_g)/T_g$, see left inset) with the $F_{1/2}$ fragility (defined in text) obtained from precise dielectric relaxation data for molecular liquids (for example, ref. 9) (filled circles) and viscosity data for inorganic compounds³ and some molecular liquids (open circles). NBS 711 and 710 are (former NBS) standard silica-based glasses, ZBLAN20 is a complex zirconium fluoride based glass, and OTP is *ortho*-terphenyl. Dashed arrows to the vertical axis show the $\Delta T_g/T_g$ of hyperquenched glassy water (HQG) and vapour-deposited glassy water (ASW), the minimum values of which were determined as shown in the right inset, following ref. 21 (T_c is the temperature at which the glass transition is cut short by crystallization). Comparison with the value for SiO_2 , or reference to the correlation line for all systems, identifies vitreous water as a very 'strong' liquid. The $\Delta T_g/T_g$ values obtained from the curves in the right inset are minimum values because (1) the annealing treatment used by Hallbrucker *et al.*²¹ to sharpen the glass transition usually reduces its width, and (2) crystallization may have occurred before the transition was complete. The correlation line in is a relation between $\Delta T_g/T_g$ and $F_{1/2}$ calculated using the methodology of ref. 3, which assumes that the temperature dependence of τ or η can be reasonably approximated by the Vogel–Tammann–Fulcher equation. In addition, it was assumed in the calculation that τ and η change by 16 orders of magnitude between T_g and their high temperature limits and by 2.3 orders of magnitude between T_g and T'_g , from which we derive $\Delta T_g/T_g = 0.151(1 - F_{1/2})(1 + F_{1/2})$. Because these assumptions are valid only to varying degrees of approximation for different liquids, the scatter of the data points about the correlation line is expected.

glass)^{20,21}, because, in this path to the glass, the sample is continuously liquid. However the findings are much the same for other amorphous waters, such as vapour-deposited amorphous solid water (ASW), as seen in Fig. 2, right inset. The differential scanning calorimetry (DSC) data for HQG and ASW, after an annealing treatment to remove the excess enthalpy frozen-in during the hyperquench (followed by further annealing below T_g to enhance the transition strength to a detectable level²¹), are shown in Fig. 2, right inset. The reduced-width $\Delta T_g/T_g$ found is 0.10 and is remarkably large—as large as that of the archetypal strong liquid, SiO₂. This reduced-width value is marked by a horizontal dashed arrow in Fig. 2. From comparison with the $\Delta T_g/T_g$ for silica or from the intersection with the $\Delta T_g/T_g$ versus $F_{1/2}$ correlation line, the $F_{1/2}$ value for low-temperature liquid water is seen to be very small. Indeed, taking the thermal treatment into account (see Fig. 2 legend), this water must be the strongest liquid yet identified. In this sense, it is quite distinct as a liquid from the water observed above 230 K (see Fig. 1).

Whereas the reduced- T_g -width approach that we have used here is the most direct way at present available of identifying HQG water as a ‘strong’ liquid, there are several ways of supporting this conclusion, though they cannot be detailed here. One is from the enthalpy relaxation activation energy of ~ 50 kJ mol⁻¹ cited by Hofer *et al.*²³, which translates via simple equations to $F_{1/2} \approx 0.05$. Another invokes the thermodynamic fragility introduced earlier by comparing the tiny value (1.6 J mol⁻¹ K⁻¹; ref. 21) of the excess heat capacity ($C_p(\text{liq.}) - C_p(\text{glass})$) measured across the glass transition (Fig. 2 insert) with the very large value for supercooled water above 236 K (ref. 14).

Thus the difference in character of water above 236 K and below 150 K, that is, in the observable ranges, is real and extreme. So what is implied about the events occurring in water during continuous, if very fast, cooling from normal temperatures?

To answer this we turn to the second of the two possibilities discussed with equal weight by Speedy and Angell in their original analysis of the apparently divergent properties of supercooled water²⁴. As an alternative to the much-discussed, and now disputed, stability limit interpretation²⁴ (which corresponds to the system reaching the ‘edge’ of its free-energy surface, $G(P,T)$) Speedy and Angell proposed that running across this surface might be a ridge associated with an end-point in the open hydrogen-bonded network formation process. This process was seen as “geometrically cooperative”²⁴, which would give rise to a region of rapid entropy change. Expected would be a peak in the heat capacity, followed by a drop to very small excess heat capacity, due to the exhaustion of the network degrees of freedom—as envisaged in ref. 14. The existence of an extremum in compressibility has been shown²⁵ to be a thermodynamic consequence of the existence of a density maximum, and must be observed in water somewhat below 4 °C unless pre-empted by some other phenomenon. Possible pre-emptives would be a first-order phase transition, as seen in liquid silicon^{26,27}, or the glass transition, as observed in liquid SiO₂ (ref. 28), below their respective ambient-pressure density maxima.

Theory²⁹ shows C_p extrema must also occur, but not necessarily at the same temperature as that of the compressibility maximum. However, an analysis³⁰ of available thermodynamic data constrains the C_p maximum to lie fairly close to 228 K, if the changes are to be continuous. Below such a maximum, the C_p of water must fall to the low value observed, and then the Adam–Gibbs equation³¹—which has so far proved quite successful for liquids near their T_g (refs 9, 32)—would require the liquid to be ‘strong’ in character.

The Adam–Gibbs theory connects the temperature dependence of the relaxation time or of a related transport property to the variation with temperature of the configurational entropy S_c via the relation

$$\tau = \tau_0 \exp(C/T S_c) \quad (1)$$

where τ_0 and C are constants. It has been shown³³ to describe well the anomalously large and non-Arrhenius temperature dependence of the diffusion coefficient of water above 243 K. Near T_g , with almost no heat capacity in excess of the vibrational component, equation (1) would predict very different behaviour. S_c would be almost constant, and an Arrhenius temperature dependence of transport properties corresponding to a ‘strong’ liquid, as indicated in the present work, would be found for any relaxation or transport process coupled to the entropy fluctuations responsible for the C_p behaviour. Thus the fragile-to-strong liquid transition on cooling is intimately connected to the presence of a thermodynamic event in liquid water. We note that near a critical point in a two-component liquid, self-diffusivity does not follow viscosity or mutual diffusion³⁴, so it is possible that the diffusivity^{35,36} of water could, as a decoupled background mode, be an exception to these expectations.

Inverting the analysis of ref. 26, Roberts *et al.*³⁷ recognize that the thermodynamic event in water referred to above would require a density extremum at a higher temperature. Hence this event could account for the existence of the density maximum of water at 4 °C. □

Received 29 December 1998; accepted 26 January 1999.

- Angell, C. A. Relaxation in liquids, polymers and plastic crystals—strong/fragile patterns and problems. *J. Non-Cryst. Solids* **131**–133, 13–31 (1991).
- Angell, C. A. Formation of glasses from liquids and biopolymers. *Science* **267**, 1924–1935 (1995).
- Moynihan, C. T. Correlation between the width of the glass transition and the temperature dependence of the viscosity in high T_g glasses. *J. Am. Ceram. Soc.* **76**, 1081–1087 (1993).
- Kauzmann, W. The nature of the glassy state and the behavior of liquids at low temperatures. *Chem. Rev.* **43**, 219–256 (1948).
- Angell, C. A. & Tucker, J. C. Heat capacities and fusion entropies of the tetrahydrates of calcium nitrate, cadmium nitrate, and magnesium acetate. Concordance of calorimetric and relaxational ‘ideal’ glass transition temperatures. *J. Phys. Chem.* **78**, 278–281 (1974).
- Xu, Y. & Hepler, L. Calorimetric investigations of crystalline, molten, and supercooled Ca(NO₃)₂·4H₂O and of concentrated Ca(NO₃)₂(aq). *J. Chem. Thermodyn.* **25**, 91–97 (1993).
- Angell, C. A. *et al.* Liquid fragility and the glass transition in water and aqueous solutions. *Int. J. Food Sci.* **22**, 115–142 (1994).
- Takahara, S., Yamamoto, O. & Matsuo, T. Calorimetric study of 3-bromopentane: correlation between structural relaxation time and configurational entropy. *J. Phys. Chem.* **99**, 9589–9592 (1995).
- Richert, R. & Angell, C. A. Dynamics of glass-forming liquids. IV: On the link between molecular dynamics and configurational entropy. *J. Chem. Phys.* **108**, 9016–9026 (1998).
- Chang, S. S. & Bestul, A. b. Heat capacities of selenium crystal (trigonal), glass, and liquid from 5 to 360 K. *J. Chem. Thermodyn.* **6**, 325–344 (1974).
- Gibbs, J. H. in *Modern Aspects of the Vitreous State* (ed. McKenzie, J. D.) Ch. 7 (Butterworths, London, 1960).
- Goldstein, M. Viscous liquids and the glass transition. IV. Thermodynamic equations and the transition. *J. Phys. Chem.* **77**, 667–673 (1973).
- Sastry, S., Debenedetti, P. G. & Stillinger, F. H. Signatures of distinct dynamical regimes in the energy landscape of a glass-forming liquid. *Nature* **393**, 554–557 (1998).
- Angell, C. A., Shuppert, J. & Tucker, J. C. Anomalous properties of supercooled water: heat capacity, expansivity, and PMR chemical shift from 0 to –38 °C. *J. Phys. Chem.* **77**, 3092–3099 (1973).
- Donth, E. The size of cooperative rearranging region at the glass transition. *J. Non-Cryst. Solids* **53**, 325–330 (1982).
- Hodge, I. M. Comment on the fragility of liquids—a brief critique. *J. Non-Cryst. Solids* **202**, 164–172 (1997).
- Angell, C. A. Simple glassformers: their definition, fragilities and landscape excitation profiles. *J. Phys., Cond. Matter* **11**, 75–94 (1999).
- Angell, C. A. & Sare, E. J. Glass-forming composition regions and glass transition temperatures for aqueous electrolyte solutions. *J. Chem. Phys.* **52**, 1058–1068 (1970).
- Angell, C. A. & Tucker, J. C. Heat capacity changes in glass-forming aqueous solutions, and the glass transition in vitreous water. *J. Phys. Chem.* **84**, 268–272 (1980).
- Johari, G., Hallbrucker, A. & Mayer, E. The glass-liquid transition of hyperquenched water. *Nature* **330**, 552–553 (1987).
- Hallbrucker, A., Mayer, E. & Johari, G. P. Glass-liquid transition and the enthalpy of devitrification of annealed vapor-deposited amorphous water. A comparison with hyperquenched glassy water. *J. Phys. Chem.* **93**, 4986–4990 (1989).
- Angell, C. A., Clarke, J. H. R. & Woodcock, L. V. Interaction potentials and glass formation: A survey of computer experiments. *Adv. Chem. Phys.* **48**, 397–453 (1981).
- Hofer, K., Mayer, E. & Johari, G. P. Glass-liquid transition of water and ethylene glycol solution in poly(2-hydroxyethyl methacrylate) hydrogel. *J. Phys. Chem.* **94**, 2689–2696 (1990).
- Speedy, R. J. & Angell, C. A. Isothermal compressibility of supercooled water and evidence for a thermodynamic singularity at 45 °C. *J. Chem. Phys.* **65**, 851–858 (1976).
- Sastry, S., Debenedetti, P. G., Sciortino, F. & Stanley, H. E. Singularity-free interpretation of the thermodynamics of supercooled water. *Phys. Rev. E* **53**, 6144–6154 (1996).
- Thompson, M. O., Galvin, G. J. & Mayer, J. W. Melting temperatures and explosive crystallization of amorphous silicon during pulsed laser irradiation. *Phys. Rev. Lett.* **52**, 2360–2363 (1984).
- Angell, C. A. & Borick, S. Comment on “Structure of Supercooled Liquid Silicon” by Ansell *et al.* *J. Phys., Cond. Matter* (in the press).
- Brückner, R. Metastable equilibrium density of hydroxyl-free synthetic vitreous silica. *J. Non-Cryst. Solids* **5**, 281–285 (1971).
- Rebelo, L. P. N., Debenedetti, P. G. & Sastry, S. Singularity-free interpretation of the thermodynamics of supercooled water. II. Thermal and volumetric behavior. *J. Chem. Phys.* **109**, 626–633 (1998).
- Starr, F., Angell, C. A., Speedy, R. J. & Stanley, H. E. Entropy and dynamic properties of water at 1 atm in the “experimentally-inaccessible” region between 150K and 236K. *Phys. Rev. Lett.* (submitted).
- Adam, G. & Gibbs, J. H. On the temperature dependence of cooperative relaxation properties in glass-forming liquids. *J. Chem. Phys.* **43**, 139–146 (1965).
- Angell, C. A. Entropy and fragility in supercooling liquids. *J. Res. NIST* **102**, 171–185 (1997).
- Angell, C. A., Finch, E. D., Woolf, L. A. & Bach, P. Spin-echo diffusion coefficients of water to 2380 bar and –20 °C. *J. Chem. Phys.* **65**, 3063–3066 (1976).

34. Allegra, J. C., Stein, A. & Allen, G. F. Tracer diffusion and shear viscosity for the system isobutyric acid-water near the critical mixing point. *J. Chem. Phys.* **55**, 1716–1720 (1971).
35. Smith, R. S., Huang, C. & Kay, B. D. Evidence for molecular translational diffusion, during the crystallization of amorphous solid water. *J. Phys. Chem. B* **101**, 6123–6126 (1997).
36. Smith, R. S. & Kay, B. D. Evidence for the existence of supercooled liquid water at 150 K. *Nature* **398** (in the press)
37. Roberts, C. J., Karayiannakis, C. & Debenedetti, P. G. Liquid-liquid immiscibility in single-component network-forming fluids: Model calculations and implications for polyamorphism in water. *Ind. Eng. Chem. Res.* **37**, 3012–3022 (1998).

Acknowledgements. This work was supported by the NSF DMR Solid State Chemistry program.

Correspondence and requests for materials should be addressed to C.A.A. (e-mail: caa@asu.edu).

Control of crystal nucleation by patterned self-assembled monolayers

Joanna Aizenberg*, Andrew J. Black† & George M. Whitesides†

* Bell Laboratories, Lucent Technologies, Murray Hill, New Jersey 07974, USA

† Department of Chemistry and Chemical Biology, Harvard University, Cambridge, Massachusetts 02138, USA

An important requirement in the fabrication of advanced inorganic materials, such as ceramics and semiconductors, is control over crystallization^{1–4}. In principle, the synthetic growth of crystals can be guided by molecular recognition at interfaces^{5–16}. But it remains a practical challenge to control simultaneously the density and pattern of nucleation events, and the sizes and orientations of the growing crystals. Here we report a route to crystal formation, using micropatterned self-assembled monolayers^{17,18}, which affords control over all these parameters. We begin with a metal substrate patterned with a self-assembled monolayer having areas of different nucleating activity—in this case, an array of acid-terminated regions separated by methyl-terminated regions. By immersing the patterned substrates in a calcium chloride solution and exposing them to carbon dioxide, we achieve ordered crystallization of calcite in the polar regions, where the rate of nucleation is fastest; crystallization can be completely suppressed elsewhere by a suitable choice of array spacing, which ensures that the solution is undersaturated in the methyl-terminated regions. The nucleation density (the number of crystals formed per active site) may be controlled by varying the area and distribution of the polar regions, and we can manipulate the crystallographic orientation by using different functional groups and substrates.

We patterned self-assembled monolayers (SAMs) on the metal substrates by microcontact printing with an elastomeric stamp^{18,19} that had a relief structure consisting of a square array of raised circles with diameter d and periodicity p (Fig. 1a): as “inks”, we used 10 mM solutions of $\text{HS}(\text{CH}_2)_n\text{X}$ ($\text{X} = \text{CO}_2\text{H}$, SO_3H , OH) in ethanol. The surface was then washed with a 10 mM solution of $\text{HS}(\text{CH}_2)_{15}\text{CH}_3$ in ethanol to passivate the areas that had not contacted the stamp. We focus on the crystallization of calcite (CaCO_3). The general principles of calcite formation have been extensively studied, due to the importance of this mineral in nature as a structural material^{20,21}. The patterned substrates were supported upside-down in a calcium chloride solution to ensure that only particles grown on the SAM would be bound to the surface, and placed in a closed desiccator with vials of solid ammonium carbonate in the bottom⁶ (Fig. 1b).

The surfaces decorated with crystals were examined using a scanning electron microscope (SEM) operating at 15 keV. The crystallographic orientations of the crystals relative to the surface were determined using X-ray diffraction and morphological

analysis²⁰. Figure 1c shows a low-magnification micrograph of the pattern of calcite crystals formed on a sample SAM—printed 35- μm circles of $\text{HS}(\text{CH}_2)_{15}\text{CO}_2\text{H}$ in a background of $\text{HS}(\text{CH}_2)_{15}\text{CH}_3$ —supported on Ag ($[\text{Ca}^{2+}] = 25 \text{ mM}$, crystallization time $t = 30 \text{ min}$). Crystallization is restricted to well defined, CO_2^- -terminated regions, and does not occur on the CH_3 -terminated area of patterned surfaces, although the solution was supersaturated in CaCO_3 and crystal formation occurred on both CO_2^- - and CH_3 -terminated SAMs when they were not patterned (Fig. 1c, insets).

By adjusting the pattern, density and sizes of features in the stamp, the concentration of the crystallizing solution, and the

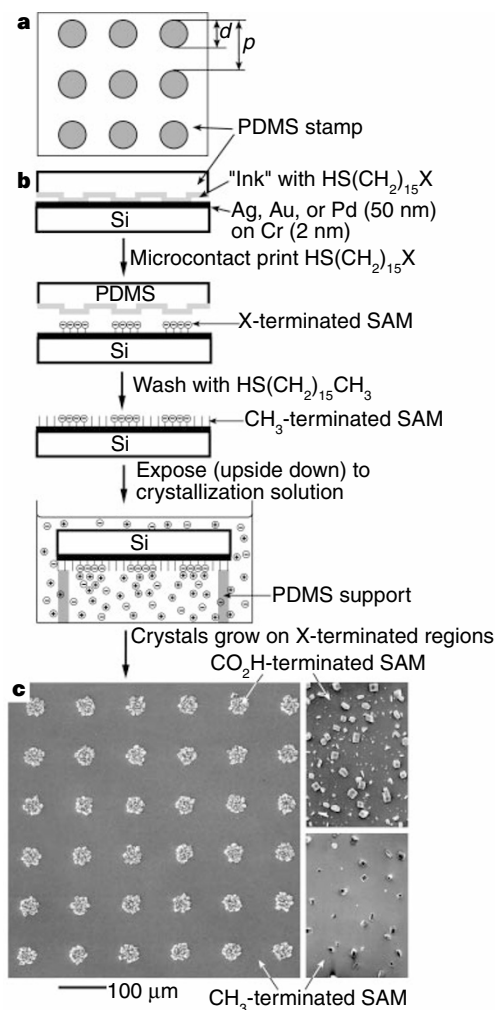


Figure 1 Experimental design of crystallization on patterned SAMs. **a**, Relief structure of the patterned PDMS stamps used for microcontact printing. **b**, Schematic presentation of the experimental steps. Dimensions are not to scale. **c**, Scanning electron micrograph (SEM) of the sample patterned surface—printed circles of $\text{HS}(\text{CH}_2)_{15}\text{CO}_2\text{H}$ in a background of $\text{HS}(\text{CH}_2)_{15}\text{CH}_3$ supported on Ag(111)—overgrown with calcite crystals. For these experimental conditions— $[\text{Ca}^{2+}] = 25 \text{ mM}$, $\text{pH} \sim 7$, crystallization time $t = 30 \text{ min}$ —the nucleation is highly specific to the acid-terminated regions, and the crystals are remarkably uniform in size and nucleation density. The insets illustrate the wide distribution of sizes of crystals formed on the non-patterned SAMs presenting the same terminal groups to a solution with the same value of $[\text{Ca}^{2+}]$. To prepare substrates, silicon wafers (test grade, n or p type, Silicon Sense, Nashua, NH) were coated with 2.5 nm of Cr, to promote adhesion, and then with metal (Ag, Au, Pd; typically $\sim 50 \text{ nm}$) using an electron beam evaporator (base pressure 10^{-7} torr). The stamps were prepared by casting and curing poly(dimethylsiloxane) (PDMS) against rigid masters bearing a photoresist pattern formed using conventional lithographic techniques^{18,19}. Calcite crystals formed on diffusion of carbon dioxide and ammonia vapours into the CaCl_2 solution.